# Plasmon-enhanced nonlinear yield in the Otto and Kretschmann configurations

Jan Heckmann,[1] Karsten Pufahl,[1] Philipp Franz,[1] Nicolai B. Grosse,[1] Xiaoqin Li,[2] and Ulrike Woggon[1]
[1]*Institut für Optik und Atomare Physik, Technische Universität Berlin, Straße des 17. Juni 135, 10623 Berlin, Germany*
[2]*Department of Physics, The University of Texas at Austin, Austin, Texas 78712, USA*

(Received 3 April 2018; revised manuscript received 8 August 2018; published 7 September 2018)

Propagating surface plasmons in the laboratory can have basic properties quite different from those of the ideal surface plasmon polariton, which is a bound mode at the interface between two infinite media. Features such as field confinement and propagation length are affected by the configuration used for coupling to the far field. We experimentally investigate how the Otto and Kretschmann configurations influence the linear coupling properties of smooth metal layers and the nonlinear generation of the second harmonic. The results are compared to calculations from electrodynamic theory based on the hydrodynamic model, which confirm that the nonlinear yield is an order of magnitude greater in the Kretschmann configuration than in the Otto configuration.

DOI: 10.1103/PhysRevB.98.115415

## I. INTRODUCTION

Surface plasmon polaritons (SPs) have been known as solutions of Maxwell's equations since the work of Zenneck and Sommerfeld [1,2]. Perhaps their simplest manifestation occurs at the planar interface between a conductor and a dielectric, where the evanescently confined electromagnetic field is coupled to plasma oscillations in the conductor. Excitation of SPs via the method of attenuated total internal reflection (ATR) was first demonstrated by Otto [3], closely followed by Kretschmann and Raether, who developed an alternative ATR configuration [4].

Relevant to the nonlinear optical properties of conductors, in the same year as Otto and Kretschmann and Raether, Bloembergen *et al.* published a work on second-harmonic generation (SHG) in reflection from media with inversion symmetry [5]. Although not explicitly considering SPs, they showed that centrosymmetric materials (e.g., noble metals) effectively have their symmetry broken at the surface, thereby allowing SHG to no longer be solely dependent on the gradient of the electric field but also on the electric field strength itself.

Since SPs exhibit confinement of the electromagnetic field at a metal-dielectric interface, large field strengths and gradients can result there, enhancing the SHG [6]. This has led to the rapidly developing field of nonlinear plasmonics [7–12]. Alternatively, the yield of SHG can also be employed as a probe of plasmonic resonances and field enhancement [13]. Such enhancements have provided the basis for the application of SPs in optical sensing, optical modulation, and the development of photovoltaic systems and are also responsible for boosting the yield of other nonlinear optical processes such as surface-enhanced Raman scattering [14–18].

To gain insight into the field enhancement properties of SPs and to understand the nonlinear sources of polarization leading to SHG, one can turn to the ATR coupling configurations which excel in their coupling of the SP mode to the far field. However, due to difficulties in practice, the Otto configuration has been much less represented in the experimental literature than the Kretschmann configuration, despite its advantages of a tunable coupling efficiency and compatibility with bulk samples.

In this paper we investigate the two basic ATR coupling configurations and consider their similarities and differences. We present a comparison of absolute values for the SHG yield from samples in the Otto and Kretschmann configurations and calculations of those yields within the hydrodynamic model. In a study of SPs excited in the Otto configuration on bulk gold, we obtain ATR curves and SHG yield as a function of coupling efficiency, as varied by adjusting the air gap. As a control, a series of samples was prepared in the Kretschmann configuration with a range of metal thicknesses, leading to a range of coupling efficiencies, and their ATR curves and SHG yields were similarly measured. While we find that both configurations can theoretically lead to perfect in-coupling efficiencies for incident plane waves, there are significant differences in the SHG fields radiated.

Our experimental results are supported by a calculation based on the hydrodynamic model, which gives insight into the nonlinear polarization for both bulk ("forbidden") and surface ("allowed") contributions. The differences between the harmonic conversion efficiencies of the two configurations can be explained by attention to the source terms driven by the fundamental field and to the out-coupling efficiencies for the second harmonic.

We give an estimate of the nonlinear conversion parameters established by Rudnick and Stern [19] and expanded by Sipe *et al.* [20] by comparing the measured conversion efficiencies to the predictions of the hydrodynamic model. Finally, we analyze both true and apparent resonances below and on the light line, as evidenced by their nonlinear signature [21].

## II. THEORY

Direct excitation of a SP at a metal/dielectric interface by light incident from the dielectric is impossible because for such incident light the wave-vector component in the plane of the interface $\kappa$ cannot reach $k_{SP}$, the magnitude of the wave vector of the surface plasmon. Achieving a $\kappa$ that reaches $k_{SP}$ can be done by using diffraction gratings or appropriate excitation scenarios that can provide an enhanced wave-vector

 

component. Essential for both the Otto and Kretschmann configurations is ATR, in which an evanescent wave results by way of total internal reflection of light incident from a medium with a greater refractive index onto one with a lower refractive index. This evanescent wave in the low-index medium has a larger in-plane wave-vector component than what can be attained by a propagating wave in the same medium. We are interested in SPs at an air/metal interface, and the total reflection that is attenuated occurs at a glass/air interface, with light incident from the glass. The SP can be excited by tuning the incident angle $\theta$ of light at frequency $\omega$ in the glass so that the in-plane component of the incident wave vector $\kappa = k_0\sqrt{\varepsilon_g}\sin\theta$ reaches $k_{\mathrm{SP}}$. Here, $\varepsilon_g$ is the relative dielectric constant of the glass at $\omega$, and $k_0 = \omega/c$, with $c$ being the light velocity in vacuum. For an isolated air/metal interface

$$k_{\mathrm{SP}} = k_0\sqrt{\frac{\varepsilon_m\varepsilon_a}{\varepsilon_m+\varepsilon_a}}, \tag{1}$$

where $\varepsilon_a$ and $\varepsilon_m$ are the relative dielectric constants of the air and metal, respectively, at frequency $\omega$. The actual $k_{\mathrm{SP}}$ differs from the nominal expression (1) because of the presence of neighboring interfaces. While $k_{\mathrm{SP}}$ has an imaginary part due to the loss in the metal [even in the limit of (1)], it also acquires an imaginary part due to the coupling of energy via these very neighboring interfaces. Under some conditions the SP resonances and propagation properties are strongly modified by the neighboring dielectric environment, which can in some situations also support additional modes [12,21]. In addition, intrinsic SP mode properties are particularly sensitive to surface roughness and contamination of the metal surface, both of which significantly affect the SP's wave-vector, lifetime, and resonant field enhancement.

For our two configurations we consider a two-dimensional structure with three layers for the Kretschmann configuration and four layers for the Otto configuration (see Fig. 1). The plane of incidence is chosen to be the $xz$ plane. The Otto configuration consists of a BK7 glass coupling prism ($M_1$) followed by an air gap ($M_2$) with an adjustable thickness $D_2$, which is used to vary the coupling to SPs on the gold-air interface. Therefore, a thick gold film ($M_4$) was thermally deposited on a glass substrate ($M_3$), resulting in the order

$$\begin{array}{rcccl} z & > & D_2 & \text{glass} & M_1 \text{ with } \varepsilon_1 = \varepsilon_g, \\ D_2 & > z > & 0 & \text{air} & M_2 \text{ with } \varepsilon_2 = \varepsilon_a, \\ 0 & > z > & -D & \text{gold} & M_4 \text{ with } \varepsilon_4 = \varepsilon_m, \\ & z < & -D & \text{substrate} & M_3 \text{ with } \varepsilon_3 \end{array}$$

for the Otto configuration.

The Kretschmann configuration is based on the same principle, but the layer order is inverted. The coupling prism ($M_1 = M_2$) is directly followed by a thin gold film ($M_4$) which was thermally deposited. SPs can be excited at the interface between the metal and the surrounding dielectric ($M_3$), which is air in this case. The arrangement in the Kretschmann configuration thus is

$$\begin{array}{rcccl} z & > & 0 & \text{glass} & M_1 \text{ with } \varepsilon_1 = \varepsilon_g, \\ 0 & > z > & -D & \text{gold} & M_4 \text{ with } \varepsilon_4 = \varepsilon_m, \\ & z < & -D & \text{air} & M_3 \text{ with } \varepsilon_3 = \varepsilon_a. \end{array}$$

The coupling to SPs requires $p$-polarized excitation, so we limit our consideration to this polarization, and we define

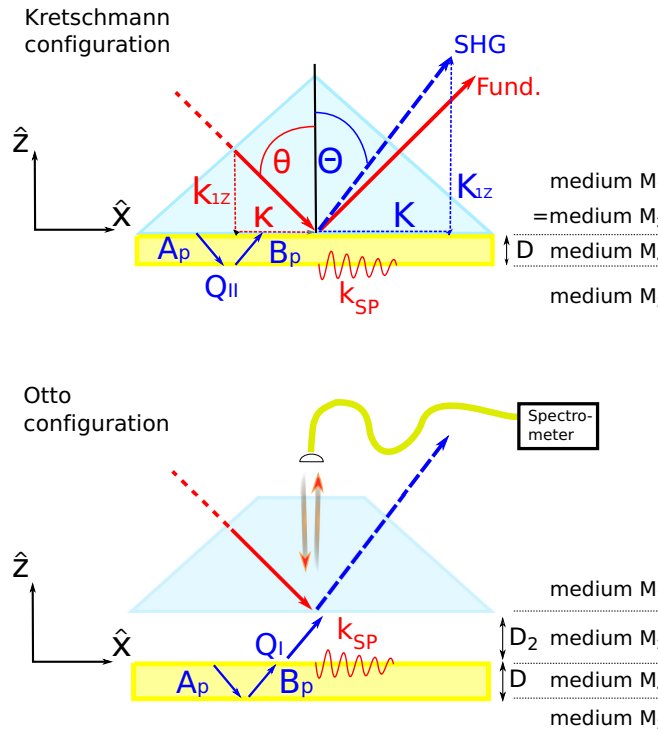


FIG. 1. Excitation configurations. The top image shows the Kretschmann configuration consisting of a glass prism and a gold layer with thickness of the order of $\lambda/10$, surrounded by air. The bottom image shows the Otto configuration composed of a glass prism, an air gap of the order of $\lambda$, and a gold layer of a fixed thickness.

$\hat{\boldsymbol{\kappa}} = \hat{\mathbf{x}}$. The polarization vectors specifying $p$-polarized light for the fundamental ($\hat{\mathbf{p}}_{i\pm}$) and second-harmonic ($\hat{\mathbf{P}}_{i\pm}$) waves in medium $i$ are given by

$$\begin{aligned} \hat{\mathbf{p}}_{i\pm} &= \frac{\kappa\hat{\mathbf{z}} \mp k_{iz}\hat{\boldsymbol{\kappa}}}{k_0\sqrt{\varepsilon_i}}, \\ \hat{\mathbf{P}}_{i\pm} &= \frac{K\hat{\mathbf{z}} \mp K_{iz}\hat{\boldsymbol{\kappa}}}{K_0\sqrt{\mathcal{E}_i}}, \end{aligned} \tag{2}$$

where the $\pm$ in $\hat{\mathbf{p}}_{i\pm}$ and $\hat{\mathbf{P}}_{i\pm}$ identify the upward- (+) and downward- (−) propagating or evanescent fields; note $\hat{\mathbf{p}}_{i\pm}\cdot\hat{\mathbf{p}}_{i\pm} = \hat{\mathbf{P}}_{i\pm}\cdot\hat{\mathbf{P}}_{i\pm} = 1$, although in general the vectors themselves are complex. The wave-vector components parallel to the interface are continuous due to translational symmetry, while the $z$ components in the different media are

$$\begin{aligned} k_{iz} &= \sqrt{k_0^2\varepsilon_i - \kappa^2}, \\ K_{iz} &= \sqrt{K_0^2\mathcal{E}_i - K^2}. \end{aligned} \tag{3}$$

We generally use capital letters to refer to quantities at the second harmonic; hence, $K_0 = 2k_0$, $K = 2\kappa$, and $\mathcal{E}_i$ is the dielectric constant of medium $i$ at frequency $\Omega = 2\omega$. The angles $\theta$ and $\Theta$ refer, respectively, to the incident angles of the fundamental in the glass and the radiated angle of the second harmonic in the glass, with $\sin\theta = \kappa/(k_0\sqrt{\varepsilon_g})$ and $\sin\Theta = K/(K_0\sqrt{\mathcal{E}_g})$; recall the discussion after Eq. (1).

For a $p$-polarized fundamental field incident from medium $M_1$,

$$\mathbf{E_{inc}}(\mathbf{r}) = \hat{\mathbf{p}}_{1-} E^p_{1-} e^{-ik_{1z}z} e^{i\boldsymbol{\kappa}\cdot\mathbf{R}}, \tag{4}$$

where $\mathbf{R} = (x, y)$ and $E^p_{1-}$ is the electric field amplitude; the fundamental electric field in the metal layer $M_4$, $\mathbf{E_4}(\mathbf{r})$, can be determined from standard linear optics:

$$\begin{aligned}\mathbf{E_4}(\mathbf{r}) = {}& \hat{\mathbf{z}}\left(e^{-ik_{4z}z} + r^p_{43} e^{2ik_{4z}D} e^{ik_{4z}z}\right) C_z E^p_{1-} e^{i\boldsymbol{\kappa}\cdot\mathbf{R}} \\ & + \hat{\boldsymbol{\kappa}}\left(e^{-ik_{4z}z} - r^p_{43} e^{2ik_{4z}D} e^{ik_{4z}z}\right) C_\kappa E^p_{1-} e^{i\boldsymbol{\kappa}\cdot\mathbf{R}},\end{aligned} \tag{5}$$

where the coefficients

$$\begin{aligned} C_z &= \frac{\kappa}{k_0\sqrt{\varepsilon_4}} \frac{t^p_{24}}{1 - \bar{r}^p_{41} r^p_{43} e^{2ik_{4z}D}} \frac{t^p_{12} e^{ik_{2z}D_2}}{1 - r^p_{21} \bar{r}^p_{23} e^{2ik_{2z}D_2}}, \\ C_\kappa &= \frac{k_{4z}}{k_0\sqrt{\varepsilon_4}} \frac{t^p_{24}}{1 - \bar{r}^p_{41} r^p_{43} e^{2ik_{4z}D}} \frac{t^p_{12} e^{ik_{2z}D_2}}{1 - r^p_{21} \bar{r}^p_{23} e^{2ik_{2z}D_2}} \end{aligned} \tag{6}$$

are Fabry-Pérot coefficients that describe multiple reflections from the different interfaces, with

$$\begin{aligned} \bar{r}_{23} &= r_{24} + \frac{t_{24} r_{43} t_{42} e^{2ik_{4z}D}}{1 - r_{42} r_{43} e^{2ik_{4z}D}}, \\ \bar{r}_{41} &= r_{42} + \frac{t_{42} r_{21} t_{24} e^{2ik_{2z}D_2}}{1 - r_{21} r_{24} e^{2ik_{2z}D_2}}, \end{aligned} \tag{7}$$

and involve the $p$-polarized reflection and transmission Fresnel coefficients from medium $i$ to medium $j$, given by

$$r^p_{ij} = \frac{k_{iz}\varepsilon_j - k_{jz}\varepsilon_i}{k_{iz}\varepsilon_j + k_{jz}\varepsilon_i}, \quad t^p_{ij} = \frac{2\sqrt{\varepsilon_i}\sqrt{\varepsilon_j} k_{iz}}{k_{jz}\varepsilon_j + k_{jz}\varepsilon_i}. \tag{8}$$

The spatial variation of the field described above is based on the standard long-wavelength description, where the response of the metal at a position $\mathbf{r}$ depends only on the Maxwell electric field at that position. Since metals are centrosymmetric, such a model of the optical response, generalized to include nonlinearities, would not predict any second-harmonic generation. Instead, a more sophisticated model of the optical response at $\mathbf{r}$ is required, taking into account the variation of the Maxwell field over the region near $\mathbf{r}$. Such a model leads to the prediction of a generated nonlinear polarization that oscillates at $\Omega = 2\omega$,

$$\boldsymbol{\Pi}^{II}(\mathbf{r}, t) = \boldsymbol{\Pi}^{II}(\mathbf{r}) e^{-i\Omega t} + \text{c.c.} \tag{9}$$

Independent of the model considered, symmetry considerations allow the identification of the contributions to $\boldsymbol{\Pi}^{II}(\mathbf{r})$ that are of lowest order in the variation of the electric field [5]; in the bulk of a medium assumed to be isotropic we can write

$$\begin{aligned}\boldsymbol{\Pi}^{II}(\mathbf{r}) = {}& \beta\, \mathbf{E_4}(\mathbf{r}) \nabla\cdot \mathbf{E_4}(\mathbf{r}) + \gamma \nabla[\mathbf{E_4}(\mathbf{r})\cdot\mathbf{E_4}(\mathbf{r})] \\ & + \delta'[\mathbf{E_4}(\mathbf{r})\cdot\nabla]\mathbf{E_4}(\mathbf{r}),\end{aligned} \tag{10}$$

where $\{\beta, \gamma, \delta'\}$ is a set of coefficients [5] whose values must be determined from a model. Since the second-harmonic generation is weak, we take the fundamental fields $\mathbf{E_4}(\mathbf{r})$ to be those in the absence of any SHG (undepleted pump approximation) and calculated in the long-wavelength limit given above. Then, since in that limit $\nabla\cdot\mathbf{E_4}(\mathbf{r}) = 0$, in the bulk we can neglect the terms involving $\beta$, which we do henceforth.

Estimates of $\gamma$ and $\delta'$ can be derived by treating the nonlinear optical response of the bulk metal using the hydrodynamic model [20]. The nonlinearity arises from convective terms in the description of the current flow and from a "quantum pressure" modeled in a simple way that depends on the number density $n_0$ of electrons involved in the optical response. The hydrodynamic predictions for the nonlinear coefficients can be written as

$$\begin{aligned} \gamma_{\text{hyd}} &= \chi_{\text{hyd}}(\Omega) \frac{\chi_{\text{hyd}}(\omega)}{2en_0}, \\ \delta'_{\text{hyd}} &= -\chi_{\text{hyd}}(\Omega)\left(\frac{\chi_{\text{hyd}}(\omega)}{en_0} + \frac{m\omega^2 \chi^2_{\text{hyd}}(\omega)}{e^3 n_0^2}\right). \end{aligned} \tag{11}$$

Here, $-e$ is the charge of the electron, and $\chi_{\text{hyd}}(\omega)$ and $\chi_{\text{hyd}}(\Omega)$ are, respectively, the predictions of the hydrodynamic model of the metal susceptibility in the long-wavelength limit at the fundamental and second-harmonic frequencies,

$$\chi_{\text{hyd}}(\omega) = \frac{\varepsilon_{\text{hyd}}(\omega) - 1}{4\pi}, \tag{12}$$

where $\varepsilon_{\text{hyd}}(\omega)$ is the relative dielectric constant in the hydrodynamic model,

$$\varepsilon_{\text{hyd}}(\omega) = 1 - \frac{\omega_p^2}{\omega(\omega + i/\tau)}, \tag{13}$$

where $\tau$ is a relaxation time and $\omega_p$ is the plasma frequency,

$$\omega_p^2 = \frac{4\pi e^2 n_0}{m}. \tag{14}$$

For $n_0$ we take a value of $5.904\times10^{22}\,\text{cm}^{-3}$, calculated assuming an oxidation state of 1. With a relaxation time $\tau = 5\times10^{-15}$ s we can obtain a reasonably good fit of $\varepsilon_{\text{hyd}}(\omega)$ and $\varepsilon_{\text{hyd}}(\Omega)$ to the experimental dielectric constants at the fundamental (corresponding to a wavelength of 855 nm) and second harmonic, $\varepsilon_{\text{hyd}}(\omega) = -27.24 + 1.64i$ and $\varepsilon_{\text{hyd}}(\Omega) = -1.37 + 5.43i$, respectively, as extracted from ellipsometry. But the fit is not exact, so for $\gamma$ and $\delta'$ in Eq. (10) we use

$$\begin{aligned} \gamma &= \chi(\Omega) \frac{\chi(\omega)}{2en_0} \bar{\gamma}, \\ \delta' &= -\chi(\Omega)\left(\frac{\chi(\omega)}{en_0} + \frac{m\omega^2 \chi^2(\omega)}{e^3 n_0^2}\right) \bar{\delta}'. \end{aligned} \tag{15}$$

Here, $\chi(\omega)$ and $\chi(\Omega)$ are the susceptibilities that follow from the experimental dielectric constants $\varepsilon(\omega)$ and $\varepsilon(\Omega)$, respectively, and $\bar{\gamma}$ and $\bar{\delta}'$ are dimensionless constants that we will extract from our observed SHG. If the hydrodynamic model were to be correct for both the linear $\chi(\omega) \to \chi_{\text{hyd}}(\omega)$, $\chi(\Omega) \to \chi_{\text{hyd}}(\Omega)$ and nonlinear responses of the metal, we would find $\bar{\gamma} = \bar{\delta}' = 1$. If the hydrodynamic model were to be correct for both linear and nonlinear responses of the metal and the relaxation time were infinite, we would have $\bar{\delta}' = 0$.

Now we can calculate the relevant contribution from the bulk material $M_4$, which was defined to contain the nonlinear sources. The downward- and upward-propagating harmonic contributions are obtained via integration over the thickness $D$ of the metal film $M_4$:

$$\begin{aligned} A_p &= \int_{-D}^{0} e^{-iK_{4z}z'} \hat{\mathbf{P}}_{4+} \cdot \boldsymbol{\Pi}^{II}(z') dz', \\ B_p &= \int_{-D}^{0} e^{iK_{4z}z'} \hat{\mathbf{P}}_{4-} \cdot \boldsymbol{\Pi}^{II}(z') dz'. \end{aligned} \tag{16}$$

Next, we calculate the surface sources. The conventional approach in characterizing the surface source, going back to

Rudnick and Stern [19], is to put the source in vacuum just beyond the metal surface but to characterize its response in terms of the linear fields on the metal side of the interface. The effective dipole moment per unit area source is placed just outside the metal. In general, we get

$$\mathbf{Q}(\mathbf{R}) = \mathbf{Q}e^{i\mathbf{K}\cdot\mathbf{R}} = (\pm)\{\Gamma^T\hat{\boldsymbol{\kappa}}E^{\kappa}(\mathbf{R}+z_{\text{inter}}\hat{\mathbf{z}})E^z(\mathbf{R}+z_{\text{inter}}\hat{\mathbf{z}}) + \Gamma^z\hat{\mathbf{z}}[E^z(\mathbf{R}+z_{\text{inter}}\hat{\mathbf{z}})]^2\}, \tag{17}$$

where $z_{\text{inter}}$ indicates the $z$ component of the interface and the field should be evaluated on the metal side of the interface, with the source placed just outside it in vacuum. For $(\pm)$ we have $(+)$ if $\hat{\mathbf{z}}$ points from metal to vacuum (the conventional orientation, which here holds for the Otto configuration) and $(-)$ if $\hat{\mathbf{z}}$ points from vacuum to metal (which here holds for the Kretschmann configuration). We write the nonlinear parameters $\Gamma^{T,z}$ for the surface source as

$$\Gamma^T = \frac{e^3 n_0 b}{2m^2\omega^4} = \frac{m}{e^2 n_0}\chi(\Omega)\left(\frac{e}{m} - \frac{\omega^3\chi(\omega)}{en_0}\right)\chi(\omega)\bar{b},$$
$$\Gamma^z = \frac{e^3 n_0 a}{4m^2\omega^4}, \tag{18}$$

where $b$ and $\bar{b}$ are related according to

$$b = \frac{2m^3\omega^4}{e^5 n_0^2}\chi(\Omega)\left(\frac{e}{m} - \frac{\omega^3\chi(\omega)}{en_0}\right)\chi(\omega)\bar{b}. \tag{19}$$

Here, $a$ and $b$ appearing in $\Gamma^T$ and $\Gamma^z$, respectively, are the phenomenological parameters introduced by Rudnick and Stern [19] for the out-of-plane and in-plane components of the surface source. If we put $\bar{b} = -1$, then in the hydrodynamic model in the limit of an infinite relaxation time we find $b = -1$, the result of Rudnick and Stern in that limit. There is no prediction for $a$ unless the dynamics at the surface are worked out completely, as it depends on the details of the electron motion near the surface. Our approach here is to use $a$ and $\bar{b}$ as our phenomenological parameters, with $b$ determined from $\bar{b}$ according to (19) using the experimental values of $\chi(\omega)$ and $\chi(\Omega)$.

For the Kretschmann configuration and the orientation shown in the top panel of Fig. 1, $(-)$ is appropriate in (17), $z_{\text{inter}} = -D$, and we have

$$\mathbf{Q}_{\text{Kr}}(\mathbf{R} - D\hat{\mathbf{z}}) = \hat{\boldsymbol{\kappa}}\,Q^{\kappa}_{\text{Kr}}e^{i\mathbf{K}\cdot\mathbf{R}} + \hat{\mathbf{z}}Q^{z}_{\text{Kr}}e^{i\mathbf{K}\cdot\mathbf{R}}, \tag{20}$$

where

$$Q^{\kappa}_{Kr} = -\Gamma^T\left(1 - r^p_{43}\right)\left(1 + r^p_{43}\right)e^{2ik_{4z}D}C_{\kappa}C_z\left(E^p_{1-}\right)^2$$
$$Q^{z}_{Kr} = -\Gamma^z\left(1 + r^p_{43}\right)^2 e^{2ik_{4z}D}\left(C_z E^p_{1-}\right)^2.$$

For the Otto configuration shown in the bottom panel of Fig. 1, $(+)$ is appropriate in (1), $z_{\text{inter}} = 0$, and we have

$$\mathbf{Q}_{\text{Ot}}(\mathbf{R} + 0\hat{\mathbf{z}}) = \hat{\boldsymbol{\kappa}}\,Q^{\kappa}_{\text{Ot}}e^{i\mathbf{K}\cdot\mathbf{R}} + \hat{\mathbf{z}}Q^{z}_{\text{Ot}}e^{i\mathbf{K}\cdot\mathbf{R}}, \tag{21}$$

where

$$Q^{\kappa}_{Ot} = Q^{\kappa}_{Ot,\uparrow} + \bar{R}^p_{23}Q^{\kappa}_{Ot,\downarrow},$$
$$Q^{z}_{Ot} = Q^{z}_{Ot,\uparrow} + \bar{R}^p_{23}Q^{z}_{Ot,\downarrow}. \tag{22}$$

Here, the source term pointing from $M_4$ to $M_2$ and the one pointing from $M_2$ to $M_4$ and being reflected there have to be considered, resulting in

$$Q^{\kappa}_{Ot,\downarrow} = -\Gamma^T\left(1 - r^p_{43}e^{2ik_{4z}D}\right)\left(1 + r^p_{43}e^{2ik_{4z}D}\right)C_{\kappa}C_z\left(E^p_{1-}\right)^2,$$
$$Q^{z}_{Ot,\downarrow} = -\Gamma^z\left(1 + r^p_{43}e^{2ik_{4z}D}\right)^2\left(C_z E^p_{1-}\right)^2,$$
$$Q^{\kappa}_{Ot,\uparrow} = \Gamma^T(1 - r^p_{43}e^{2ik_{4z}D})(1 + r^p_{43}e^{2ik_{4z}D})C_{\kappa}C_z(E^p_{1-})^2,$$
$$Q^{z}_{Ot,\uparrow} = \Gamma^z(1 + r^p_{43}e^{2ik_{4z}D})^2(C_z E^p_{1-})^2.$$

Following the evaluation of the nonlinear sources, the radiated second-harmonic field can be calculated as

$$\mathbf{E}^{II}_{1+}(\mathbf{r}) = \left(E^{pII}_{1+}\hat{\mathbf{P}}_{1+}\right)e^{i\mathbf{K}\cdot\mathbf{R}}e^{iK_{1z}z}. \tag{23}$$

Combining Eqs. (10), (16), and (17), we obtain for the Kretschmann and Otto configurations, respectively,

$$E^{pII,\,Kr}_{1+} = \frac{T^p_{42}}{\left(1 - \bar{R}^p_{41}R^p_{43}e^{2iK_{4z}D}\right)}\left[\left(\frac{K_0}{K_{4z}}\right)\left(A_p + R^p_{43}e^{iK_{4z}D}B_p\right) + \left(\frac{K_0 T^p_{34}}{K_{3z}}\right)e^{iK_{4z}D}\left(\frac{K\left(K_0 Q^z_{Kr}\right) - K_{3z}\left(K_0 Q^{\kappa}_{Kr}\right)}{K_0\sqrt{\mathcal{E}_3}}\right)\right],$$
$$E^{pII,\,Ot}_{1+} = \frac{\bar{T}^p_{21}}{\left(1 - \bar{R}^p_{41}R^p_{43}e^{2iK_{4z}D}\right)}\left(\frac{K_0 T^p_{42}}{K_{4z}}\right)\left(A_p + R^p_{43}e^{iK_{4z}D}B_p\right) + \left(\frac{K_0\bar{T}^p_{21}}{K_{2z}}\right)\left(\frac{K\left(K_0 Q^z_{Ot}\right) - K_{2z}\left(K_0 Q^{\kappa}_{Ot}\right)}{K_0\sqrt{\mathcal{E}_2}}\right). \tag{24}$$

$\bar{T}^p_{21}$ is the harmonic Fabry-Pérot out-coupling coefficient given by

$$\bar{T}^p_{21} = \frac{T^p_{21}e^{iK_{2z}D_2}}{\left(1 - R^p_{21}\bar{R}^p_{23}e^{2iK_{2z}D_2}\right)}, \tag{25}$$

and $\bar{R}_{41}$ and $\bar{R}_{23}$ follow their respective definitions at $\omega$. For SHG efficiency, we expect the strongest influence in variations of the coupling layer's thickness, $D$ and $D_2$ respectively, as this was already theoretically analyzed by Tzeng and Lue [22] and Jensen *et al.* [23]. By comparing the different harmonic contributions, we identified the bulk term $B_p$ and the surface sources $Q^{\kappa}_{Kr}$, $Q^{\kappa}_{Ot}$ to be the dominant driving sources in both configurations. The influence of $A_p$ is much weaker in the Kretschmann configuration and negligible in the Otto configuration. $Q^z_{Ot}$ has to be treated carefully as it contains additional "waveguidelike" resonances. The different contributions are discussed in detail in Sec. IV.

## III. EXPERIMENTAL SETUP

For the experimental investigation we use a custom $k$-space spectroscopy setup (Fig. 2) which enables

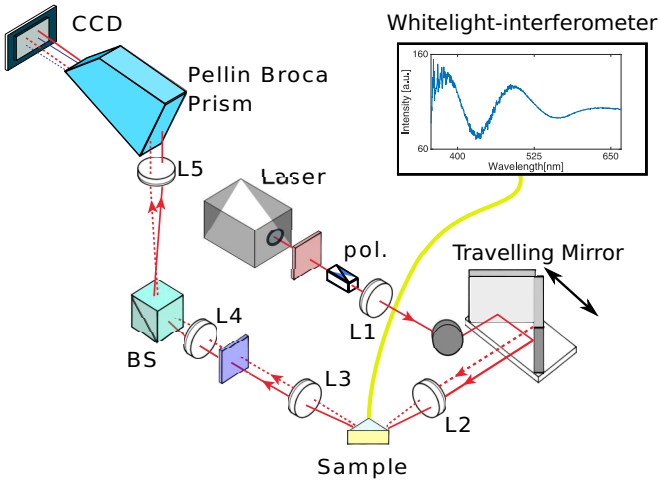


FIG. 2. Experimental setup. Mode-locked Ti:sapphire laser, pol: Glan-Taylor polarizer, L1, L2: focusing lenses, Sample: BK7 or quartz prism with gold and a dielectric layer in either the Kretschmann or Otto configuration, L3–L5: detection lenses, BS: beam splitter, a Pellin Broca prism is used to separate different wavelengths contained in the reflected light, CCD: imaging sensor.

simultaneous detection of fundamental intensity, SHG intensity, and their respective incident and exit angles [24]. A measurement of the reflected linear and nonlinear signal is realized while scanning over the plasmonic resonance. In particular, the influence of the metal layer's thickness on the conversion efficiency is studied. Our experimental setup was based on a Ti:sapphire laser with the wavelength set to 855 nm and a pulse length of 150 fs. Fluorescence from the Ti:sapphire crystal was removed by a 750-nm cut-on filter, and a Glan-Taylor polarizer was used to orientate the polarization with reference to the plane of incidence on the sample. A prefocusing lens (L1) was adjusted to position the beam's spot in the back aperture of the excitation lens (L2). The focused beam's waist on the sample was 200 $\mu$m, and the average power was 160 mW. A traveling mirror moved the spot position on the excitation lens and, consequently, the angle of incidence with respect to the prism's hypotenuse. A symmetrically arranged objective lens (L3) collected the reflected light, and a BG 40 filter was used to remove most of the fundamental intensity (optical density >9). A beam splitter (BS) was used to divide the signal, enabling the use of a monitoring camera for adjustment. The other part was transferred to a Pellin Broca prism, which separated the different wavelength components of the reflected light. A liquid-nitrogen-cooled CCD with a 1024×256 pixel array collected the light. The entire CCD array was used to detect the angular signature in the horizontal direction and the wavelength information in the vertical direction. The gold layers $M_4$ for the Kretschmann configuration were prepared between 29 and 79 nm in steps of 5 nm to investigate the influence of the layer thickness on the fundamental coupling into plasmons and the harmonic out-coupling. The gold film $M_4$ for the Otto configuration was evaporated on BK7 glass to a thickness of 200 nm. A white-light interferometer was used to control the air gap size $M_2$, which was tuned between 200 and 3000 nm.

## IV. RESULTS AND DISCUSSION

The experimental data and calculated intensities can be found in Figs. 3(a)–3(c) for the Kretschmann configuration and Figs. 3(d)–3(f) for the Otto configuration. Figure 3(a) shows the observed reflected fundamental intensity and emitted SHG in the Kretschmann configuration. A $k$-space spectrum for the relevant angular range was measured for different gold layer $M_4$ thicknesses, while keeping all other parameters constant.

In the investigated wavelength range, metal layers over 100 nm could not provide coupling to SPs, as the evanescent field did not penetrate to the relevant interface. Beginning with 79 nm Au thickness, the fundamental signal (red curve in Fig. 3(a)) was weakly coupled as a small dip of 5% was found at $\kappa/k_0 = 1.02$, which is close to the calculated ideal plasmon wave vector. A thickness reduction led to increased fundamental coupling, which was optimum at 44 nm [labeled (i) in Fig. 3(a)]. Simultaneously, the dip broadens [labeled (iii)], and its position slightly shifts to larger wave vectors. As $M_4$ is almost transparent for very thin layers, the edge of total internal reflection (TIR) $\kappa/k_0 = 1$ becomes visible. The emitted second-harmonic radiation (filled blue curve) is weakly visible starting from 64-nm layer thickness. In general, the harmonic peak follows the fundamental dip in terms of broadening [labeled (iii)] and displacement as the thickness is decreased further. On comparing the wave vectors associated with the SHG peaks and the fundamental dips, one observes only minor deviations. However, the optimal SHG yield, which is maximum at 39 nm [indicated by (ii)], is somewhat shifted to thinner layers versus the optimal coupling to the fundamental.

Our theoretical model, which includes the complete intensity from bulk [$A_p$, $B_p$ from (6)] and surface [$Q$ from (15)] sources, supports the experimental results very well. Figure 3(b) shows the calculated SHG with high resolution, and the solid lines in Fig. 3(a) are cuts for the respective metal layer thicknesses. The maximum peak position in the calculation can similarly be found around 40 nm [labeled (ii)], while broadening for thin layers is likewise visible [see (iii)]. Figure 3(c) shows the harmonic source signal at the interface ($A_p$, $B_p$, and $Q_{Kr}$) in $M_3$ (which is air) as red lines. Similar to the measurement, the field strength clearly follows the fundamental intensity. For the Kretschmann configuration, the effect of the out-coupling parameter $T_{42}^p$, plotted as grayscale shaded logarithmic contours, has a negligible effect.

Concerning the variation of the air gap in the Otto configuration, shown in Figs. 3(d)–3(f), we observed a similar behavior for the fundamental intensity. Starting at an air gap of 2.8 $\mu$m, only a small absorption feature is visible, where the nearest Fabry-Pérot mode was expected [see (iv)]. A small harmonic Fabry-Pérot contribution [labeled (v)] can be seen, which is due to the out-coupling parameter. The linear coupling strength to the fundamental SP, which theoretically lies at $\kappa/k_0 = 1.02$ for two infinite media, found a maximum [labeled (i)] around 1.2 $\mu$m. The dip broadens and slightly shifts to smaller wave vectors, contrary to the Kretschmann case. The SP-related SHG [see (ii)] rises at 0.7 $\mu$m due to the better out-coupling efficiency for this wavelength. As the air gap is reduced still further, the absorption and SHG

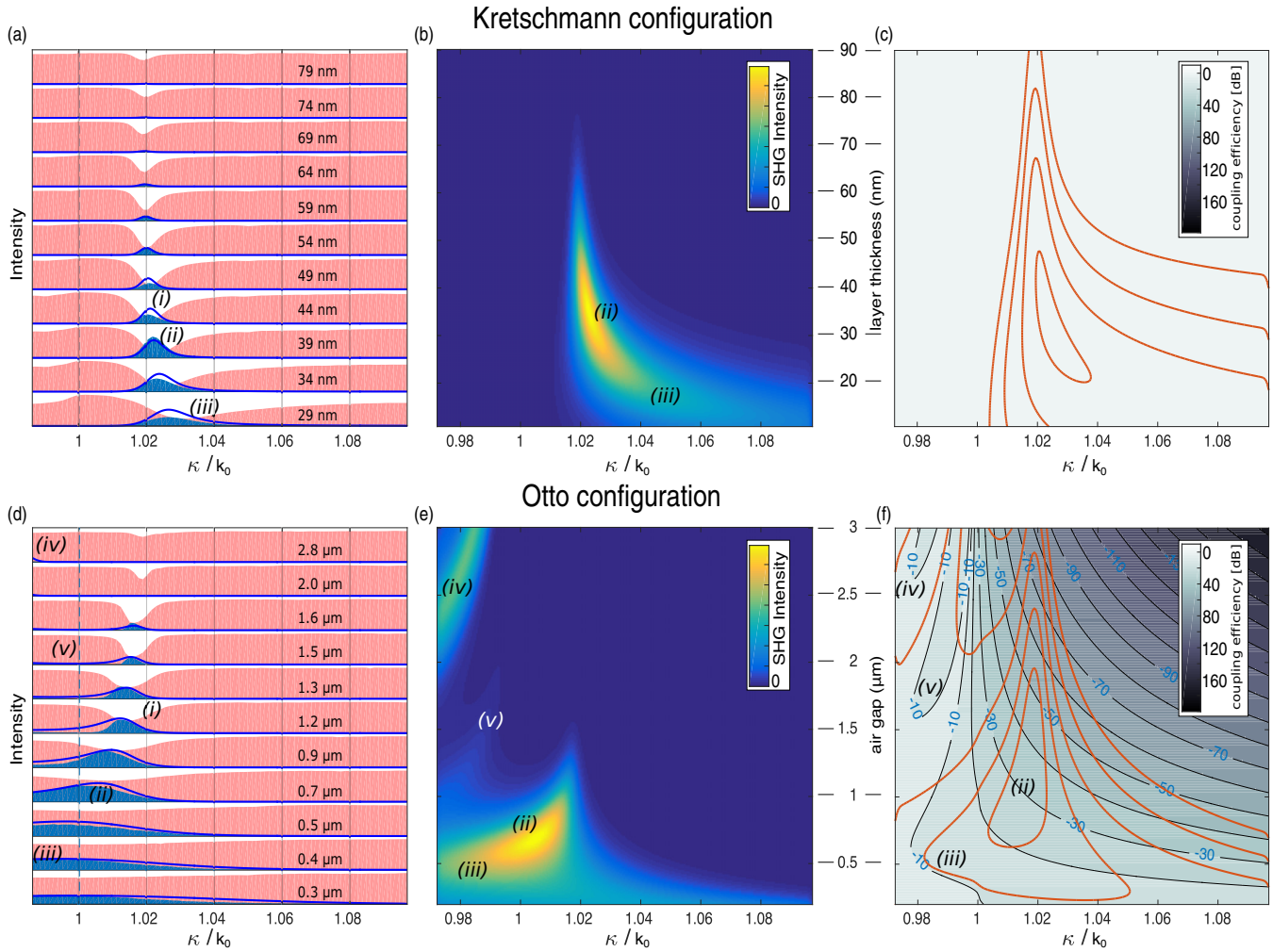


FIG. 3. (a) Experimental data for varying layer thickness in the Kretschmann configuration; red = reflected fundamental intensity, blue = emitted second-harmonic intensity, solid line = model. Here, (i) identifies the optimum coupling for the fundamental wavelength, (ii) is the maximum SHG, and (iii) marks the broadening of the coupling dip and SHG peak. (b) Theoretical calculation for SHG according to the hydrodynamic model [cuts are shown in (a) as solid lines]. (c) Calculation of the harmonic source's intensity at the metal surface (red) and the out-coupling coefficient as contours with logarithmic scale, drawn every 10 dB. (d) Experimental data for different air gaps in the Otto configuration; red = reflected fundamental intensity, blue = emitted second-harmonic intensity, solid line = model. Here, (iv) and (v) mark the fundamental and harmonic Fabry-Pérot modes, respectively. (e) Theoretical calculation for SHG according to the hydrodynamic model [cuts are shown in (d) as solid lines]. (f) Calculation of the harmonic source's intensity at the metal surface (red) and the out-coupling coefficient through the air gap and prism as contours with logarithmic scale, drawn every 10 dB.

features in $k$-space broaden [see (iii)]. Below 0.5 $\mu$m we observe the SP mode has a greatly widened resonance that spans even inside the TIR angle, where a propagating wave is expected. Evidence of strong out-coupling can be revealed if the hydrodynamic theory is considered. In Fig. 3(e) the calculated emitted harmonic radiation ($A_p$, $B_p$, and $Q_{Ot}$) is shown, which is in good agreement with the experimental data. The solid lines in Fig. 3(d) result from cuts for the respective coupling gaps. We have examined more closely the harmonic sources and individual coupling parameter to identify the cause of the broadening: Fig. 3(f) shows the nonlinear source terms from bulk and surfaces at the interface of the metallic $M_4$ and the surrounding air gap $M_2$ before coupling through air into the prism $M_1$. In contrast to the Kretschmann configuration, the out-coupling efficiency $\bar{T}_{21}^{p}$ of the Otto configuration, given by the black contour lines, strongly influences the far-field radiation. It is responsible for the large broadening [see (iii)] and the shift toward the TIR angle of the harmonic radiation's emission at small gap sizes.

In Fig. 4, the fundamental dip ratio and absolute values of second-harmonic peak powers for the Otto and Kretschmann configurations are collected to compare the harmonic yield to the fundamental coupling. It can clearly be seen that both harmonic contributions have their relative maxima in an over-coupled regime beyond impedance matching of the incident fundamental with the surface plasmon. Both configurations show up to 80% coupling efficiency for the fundamental wavelength, while the second-harmonic yield is one order of magnitude greater for the Kretschmann configuration. The harmonic signal in the Kretschmann configuration has its maximum

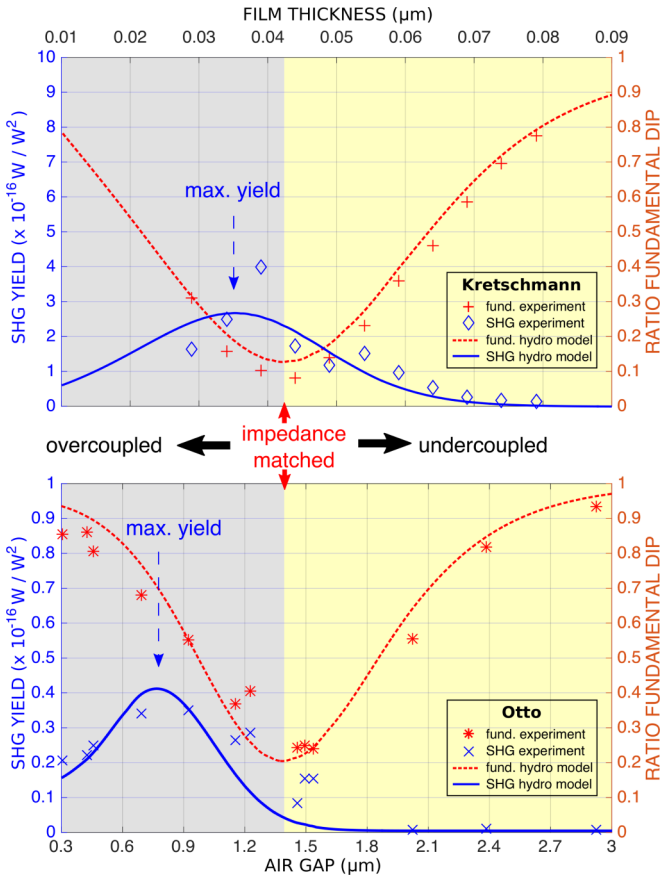


FIG. 4. Maximum SHG yield and optimal fundamental coupling as a function of metal layer thickness (Kretschmann configuration, top) and air gap variation (Otto configuration, bottom).

value at 35 nm, which is close to the fundamental optimum but already in the overcoupled regime. The hydrodynamic model matches the fundamental data for both configurations very well. For the Otto configuration, impedance matching at the fundamental wavelength is found at 1.4 $\mu$m, while the SHG maximum is located at 0.8 $\mu$m. The shift between the optimal coupling conditions for the fundamental and the harmonic is much larger for the Otto configuration than for the Kretschmann configuration. The influence of the out-coupling efficiency increases, as shown in Fig. 3(f), as the effective gap size is much larger for shorter wavelengths. Although the source SHG inside the metal $M_4$ is even stronger in the Otto configuration, the collected yield is one order of magnitude lower than in the Kretschmann configuration. This difference is reproduced by the hydrodynamic model, and the harmonic yield as a function of layer thickness is in good agreement with the experiment. The nonlinear parameters accounting for physics not included in the hydrodynamic model are obtained using the least-squares method for both configurations collectively: $\bar{\gamma} = 1, \bar{\delta}' = 1, \bar{b} = -6, a = 0.01$. The respective bounds derived from the model are $0.2 < |\bar{\gamma}| < 1.5$, $0 < |\bar{\delta}'| < 10$, $3 < |\bar{b}| < 8$, $|a| < 0.05$. All bounds are determined from a 50% deviation of the absolute nonlinear yield due to variation of the respective parameter while all other parameters are kept constant.

With this set of parameters, the hydrodynamic model reproduces the experimental observations very well. Given the sizable solution space, however, the existence of other parameter sets could be a possibility, in particular if surface roughness is considered. The bulk parameter $\bar{\gamma}$ is in good agreement with the predictions, while the parameter for the in-plane surface source $\bar{b}$ is above the expected value of the order of unity. This could be due to surface imperfections and roughness that are not contained in the model. The $\bar{\delta}'$ parameter has negligible influence in the Otto configuration and thus has a larger uncertainty. As mentioned above, there is no precise prediction for $a$. Previous publications [25] report values ranging from $-15$ to 20 and even complex values [26], both obtained from direct reflection at metal surfaces without SP excitation. In our investigation, however, the Otto configuration is much more sensitive to variations of $a$. Calculations for values larger than $a \approx 0.05$ result in an additional waveguidelike resonance at the TIR angle. Only a small contribution of this resonance was observed as broadening in the SHG signal. We can therefore limit the $a$ parameter in the case of strong contributions from the surface sources with SP excitation, which is the case in the Otto configuration, to values $|a| < 0.05$.

## V. CONCLUSION

Arguably, the mode-confinement and field-enhancement properties of SPs are their most fascinating attributes. Efficient optical access of SPs from the far field has traditionally been accomplished by using evanescent coupling in either the Otto or Kretschmann configuration. Given the similarity of their linear responses in $k$ space, it has generally been thought that both methods are equivalent. However, as we have experimentally demonstrated in this work, the second-harmonic responses in the two configurations differ markedly in their qualitative behavior (as a function of coupling strength) and quantitatively in terms of their radiated nonlinear yield.

These surprising results can be understood in terms of the nonlinear sources in the bulk metal and on the metal surfaces and how they are driven by the fundamental field and SP resonances and the limitations imposed by the out-coupling efficiency of the second harmonic to the far field. Our analysis using the hydrodynamic model of the metal film, treated in the respective configurations, confirms that the harmonic out-coupling efficiency dominates in the SHG yield from the Otto configuration, while the fundamental SP resonance governs the yield in the Kretschmann configuration.

In addition, both coupling methods also show perturbations to the fundamental's SP momentum and lifetime in the limit of strong radiative damping. In the Otto configuration these deviations from the ideal SP are caused by the strong influence of the coupling layer and SP hybridization with a photonic mode. In the Kretschmann configuration, only very thin metal layers lead to significant broadening of the resonance.

We conclude with a general observation that even though the Otto configuration is considered to be the most noninvasive method of coupling SPs to the far field, thereby guaranteeing the longest SP lifetimes and greatest field enhancements, those field enhancements do not lead to a proportionately higher yield of second-harmonic radiation. We have shown that the

hydrodynamic model enables a qualitative analysis of the experimental data as well as a quantitative calculation of the absolute second-harmonic yield. An analysis and discussion of the nonlinear parameters were given, showing that the in-plane surface source is stronger than predicted.

**ACKNOWLEDGMENTS**

We would like to thank J. E. Sipe for fruitful discussions and helpful comments. This work has been supported by the Deutsche Forschungsgemeinschaft (DFG) under Grant No. WO 477/35.

[1] J. Zenneck, Über die Fortpflanzung ebener elektromagnetischer Wellen längs einer ebenen Leiterfläche und ihre Beziehung zur drahtlosen Telegraphie, Ann. Phys. (Berlin, Ger.) **328**, 846 (1907).

[2] A. Sommerfeld, Über die Ausbreitung der Wellen in der drahtlosen Telegraphie, Ann. Phys. (Berlin, Ger.) **333**, 665 (1909)

[3] A. Otto, Excitation of nonradiative surface plasma waves in silver by the method of frustrated total reflection, Z. Phys. **216**, 398 (1968).

[4] E. Kretschmann and H. Raether, Radiative decay of nonradiative surface plasmons excited by light, Z. Naturforsch. A **23**, 2135 (1968).

[5] N. Bloembergen, R. K. Chang, S. S. Jha, and C. H. Lee, Optical second-harmonic generation in reflection from media with inversion symmetry, Phys. Rev. **174**, 813 (1968).

[6] H. J. Simon, D. E. Mitchell, and J. G. Watson, Optical Second-Harmonic Generation with Surface Plasmons in Silver Films, Phys. Rev. Lett. **33**, 1531 (1974).

[7] W. L. Barnes, A. Dereux, and T. W. Ebbesen, Surface plasmon subwavelength optics, Nature (London) **424**, 824 (2003).

[8] F. X. Wang, F. J. Rodríguez, W. M. Albers, R. Ahorinta, J. E. Sipe, and M. Kauranen, Surface and bulk contributions to the second-order nonlinear optical response of a gold film, Phys. Rev. B **80**, 233402 (2009).

[9] M. Kauranen and A. V. Zayats, Nonlinear plasmonics, Nat. Photon. **6**, 737 (2012).

[10] C.-Y. Wang, H.-Y. Chen, L. Sun, W.-L. Chen, Y.-M. Chang, H. Ahn, X. Li, and S. Gwo, Giant colloidal silver crystals for low-loss linear and nonlinear plasmonics, Nat. Commun. **6**, 7734 (2015).

[11] B. Metzger, L. Gui, J. Fuchs, D. Floess, M. Hentschel, and H. Giessen, Strong enhancement of second harmonic emission by plasmonic resonances at the second harmonic wavelength, Nano Lett. **15**, 3917 (2015).

[12] A. Delfan, I. Degli-Eredi, and J. E. Sipe, Long-range surface plasmons in multilayer structures, J. Opt. Soc. Am. B **32**, 1615 (2015).

[13] R. Naraoka, H. Okawa, K. Hashimoto, and K. Kajikawa, Surface plasmon resonance enhanced second-harmonic generation in Kretschmann configuration, Opt. Commun. **248**, 249 (2005).

[14] S. Palomba, S. Zhang, Y. Park, G. Bartal, X. Yin, and X. Zhang, Optical negative refraction by four-wave mixing in thin metallic nanostructures, Nat. Mater. **11**, 34 (2012).

[15] R. Dornhaus, R. E. Benner, R. K. Chang, R. K. Chang, and I. Chabay, Surface plasmon contribution to SERS, Surf. Sci. **101**, 367 (1980).

[16] J. Homola, S. S. Yee, and G. Gauglitz, Surface plasmon resonance sensors: Review, Sens. Actuators B **54**, 3 (1999).

[17] N. B. Grosse, J. Heckmann, and U. Woggon, Nonlinear Plasmon-Photon Interaction Resolved by $k$-Space Spectroscopy, Phys. Rev. Lett. **108**, 136802 (2012).

[18] I. Razdolski, D. Makarov, O. G. Schmidt, A. Kirilyuk, T. Rasing, and V. V. Temnov, Nonlinear surface magneto-plasmonics in Kretschmann multilayers, ACS Photon. **3**, 179 (2015).

[19] J. Rudnick and E. A. Stern, Second-harmonic radiation from metal surfaces, Phys. Rev. B **4**, 4274 (1971).

[20] J. E. Sipe, V. C. Y. So, M. Fukui, and G. I. Stegeman, Analysis of second-harmonic generation at metal surfaces, Phys. Rev. B **21**, 4389 (1980).

[21] J. J. Burke, G. I. Stegeman, and T. Tamir, Surface-polariton-like waves guided by thin, lossy metal films, Phys. Rev. B **33**, 5186 (1986).

[22] C.-C. Tzeng and J. T. Lue, Nonlinear optical generation from noble metals and aluminum films in various geometric configurations, Phys. Rev. A **39**, 191 (1989).

[23] H. R. Jensen, R. Reinisch, and J. L. Coutaz, Hydrodynamic study of surface plasmon enhanced non-local second-harmonic generation, Appl. Phys. B **64**, 57 (1997).

[24] J. Heckmann, M. E. Kleemann, N. B. Grosse, and U. Woggon, The dual annihilation of a surface plasmon and a photon by virtue of a three-wave mixing interaction, Opt. Express **21**, 28856 (2013).

[25] K. A. O'Donnel and R. Torre, Characterization of the second-harmonic response of a silver-air interface, New J. Phys. **7**, 154 (2005).

[26] A. Liebsch, Second-Harmonic Generation at Simple Metal Surfaces, Phys. Rev. Lett. **61**, 1233 (1988).